PHOTON STRUCTURE AT LEP*

STEFAN SÖLDNER-REMBOLD
Universität Freiburg
Hermann-Herder-Str. 3, D-79104 Freiburg i. Br., Germany
E-mail: soldner@ruhpb.physik.uni-freiburg.de

ABSTRACT

The structure of the photon is studied in photon interactions at high energies using photons radiated by the electron and positron beams at LEP. The current status of these measurements is reviewed.

1. Introduction

The photon is one of the fundamental gauge bosons of the Standard Model. At high energies photon interactions are dominated by quantum fluctuations of the photons into fermion-antifermion pairs and into vector mesons which have the same spin-parity ($J^{PC} = 1^{--}$) as the photon. This is called photon structure. Electron-Positron collisions at LEP are an ideal laboratory for studying photon structure in interactions of quasi-real and virtual photons, testing predictions of both QED and QCD. These results are complementary to the results obtained in γp scattering at HERA.

2. Electron–Photon Scattering

If one of the scattered electrons[a] is detected (tagged), the process $e^+e^- \to e^+e^- +$ hadrons can be regarded as deep-inelastic scattering of an electron on a quasi-real photon with the cross-section

$$\frac{d^2\sigma_{e\gamma\to e+\text{hadrons}}}{dx dQ^2} = \frac{2\pi\alpha}{x\,Q^4}\left[\left(1+(1-y)^2\right)F_2^\gamma(x,Q^2) - y^2 F_L(x,Q^2)\right], \qquad (1)$$

where $Q^2 = -q^2$ is the negative four-momentum squared of the virtual photon and x and y are the usual dimensionless variables. The structure function F_2^γ is related to the sum over the parton densities of the photon. In order to identify an electron in the detector, a large tag energy E_{tag} has to be required, i.e only low values of y are accessible ($y^2 \ll 1$). The contribution of the term proportional to the longitudinal structure function F_L^γ is therefore negligible.

For measuring $F_2^\gamma(x,Q^2)$ the value of Q^2 can be well reconstructed from the energy, E_{tag}, and the angle, θ_{tag}, of the tagged electron via the relation $Q^2 \approx 2E_{\text{beam}}E_{\text{tag}}(1-\cos\theta_{\text{tag}})$. The reconstruction of $x = Q^2/(Q^2+W^2)$, however, relies heavily on the

[a] In this paper positrons are also referred to as electrons

*Invited talk given at the Ringberg Workshop on New Trends in HERA Physics, Ringberg Castle, Germany, 25-30 May 1997

measurement of the invariant mass W from the hadronic final state.

2.1. Hadronic Energy Flows

OPAL [1], ALEPH [2] and DELPHI [3] have therefore studied the hadronic energy flow $1/N \cdot \mathrm{d}E/\mathrm{d}\eta$ as a function of the pseudorapidity $\eta = -\ln\tan\theta/2$, where the sign of η is chosen in such way that the tag electron is always at negative η. OPAL has measured

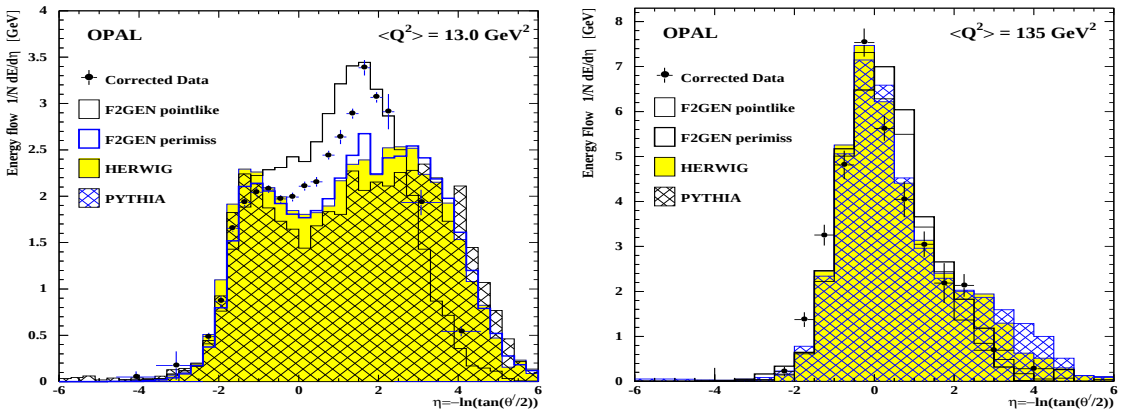

Figure 1: The energy flow per event as a function of the pseudorapidity η, compared to the HERWIG, PYTHIA and F2GEN Monte Carlo models. The data have been corrected for detector effects.

the energy flow at medium Q^2 ($\langle Q^2\rangle = 13\ \mathrm{GeV}^2$) and at high Q^2 ($\langle Q^2\rangle = 135\ \mathrm{GeV}^2$) [1]. In Fig. 1 the energy flows are compared to the two QCD based Monte Carlo generators HERWIG [4] and PYTHIA [5]. The data distributions have been corrected for detector effects. The generator F2GEN is used to model the unphysically extreme case of a two-quark state in the $\gamma^*\gamma$ centre-of-mass system with an angular distribution as in lepton pair production from two real photons ("pointlike"). The "perimiss" sample is a physics motivated mixture of pointlike and peripheral interactions, where peripheral means that the transverse momentum of the outgoing quarks is given by an exponential distribution as if all the photons interacted as pre-existing hadrons.

Significant discrepancies exist between the data and all of the Monte Carlo models. The

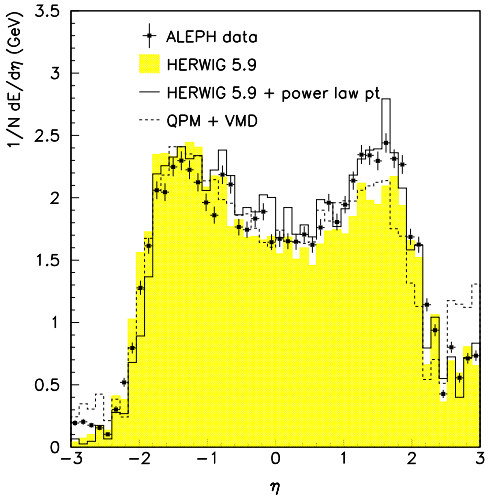

Figure 2: The energy flow per event as a function of η, compared to a QPM+VMD model, the standard and the tuned version of HERWIG.

agreement improves at higher Q^2. Since x and Q^2 are correlated, the discrepancies at low Q^2 are observed also at low x. These discrepancies between the data and the Monte Carlo model for the hadronic final state are the dominant source of systematic uncertainty in the unfolding of $F_2^\gamma(x, Q^2)$ [1].

Tuning of the Monte Carlo to improve the modelling of the hadronic final state is complicated and must be done with care in order to avoid a bias of the result of the unfolding towards the parametrisation of the parton distribution functions used in the tuned Monte Carlo. ALEPH has measured the energy flow in tagged event for $\langle Q^2 \rangle = 14.2$ GeV^2 [2]. The distributions have not been corrected for detector effects. The energy flow shown in Fig. 2 is compared to the HERWIG generator [4] and a Monte Carlo which consists of a mixture of Quark Parton Model (QPM) and Vector Meson Dominance (VMD) similar to the F2GEN generator. In addition, a modified version of HERWIG ("HERWIG+power law p_{T}") was used. The modification is based on studies of the photon remnant by ZEUS [6]. In standard HERWIG a Gaussian distribution is used to describe the limitation of the transverse momentum of the outgoing partons with respect to the initial target photon. In the modified HERWIG the Gaussian is replaced by a power law spectrum. The agreement with the data improves. A similar study was performed earlier by Lauber in Ref. 7 using OPAL data. It is expected that such improvements of the Monte Carlo models will significantly reduce the systematic error of the structure function measurements.

2.2. Photon Structure Function

The photon structure function $F_2^\gamma(x, Q^2)$ can be measured at LEP in the range $x > 10^{-3}$ and $1 < Q^2 < 10^3$ GeV^2. This will make it possible to study the QCD evolution of F_2^γ in a wide range of x and Q^2. All currently available measurements of the photon structure function are shown in Fig. 3 [8]. The data are compared to the next-to-leading order (NLO) GRV parametrisation [9] and the leading order (LO) SaS-1D parametrisation [10].

For low x and not too small Q^2 a rise of the photon structure function is expected, similar to the rise of the proton structure function observed at HERA. An interesting new F_2^γ measurement is presented by OPAL in the x and Q^2 ranges $2.5 \times 10^{-3} < x < 0.2$ and $1.1 < Q^2 < 6.6$ GeV^2. The measurements is consistent with a possible rise within large systematic errors. It should also be noted that the OPAL points tend to be significantly higher than the previous measurement by TPC/2γ in a similar kinematic range.

For large x and asymptotically large Q^2 the value of F_2^γ can be calculated from perturbative QCD due to the pointlike coupling of the photon to $\mathrm{q\overline{q}}$ pairs [11]. The next-to-leading order (NLO) result [12] can be written as

$$\frac{F_2^\gamma}{\alpha} = \frac{a(x)}{\alpha_s(Q^2)} + b(x), \tag{2}$$

where $a(x)$ and $b(x)$ are calculable functions which diverge for $x \to 0$. The first term corresponds to the LO result by Witten [11]. The measurement of F_2^γ could be a direct measurement of $\Lambda_{\rm QCD}$ if it were not for the large non-perturbative contributions due to bound states. These contributions are large at all experimentally accessible values of Q^2.

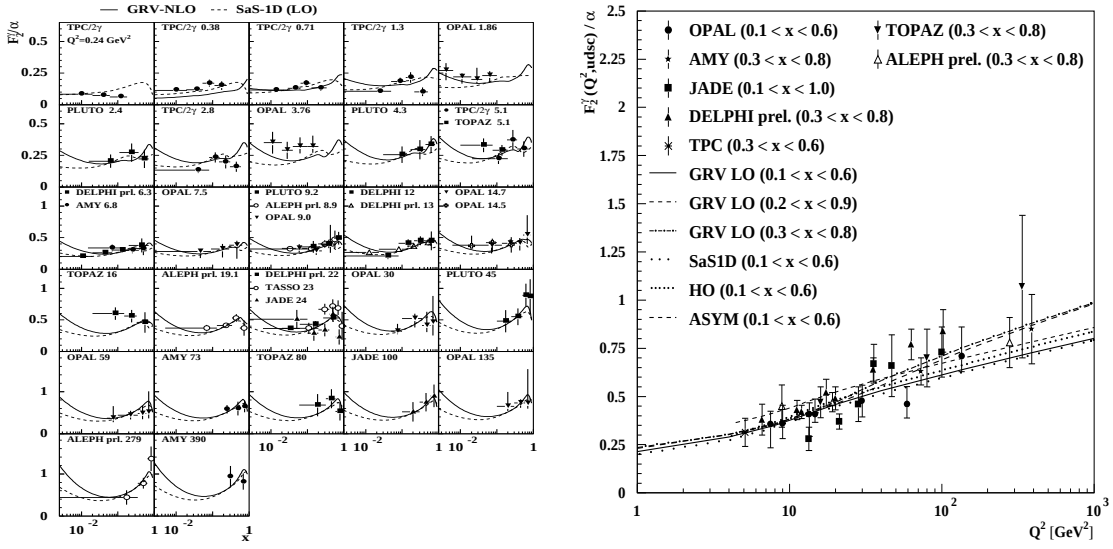

Figure 3: Measurements of the photon structure function F_2^γ in bins of x and Q^2.

The evolution of F_2^γ with $\ln Q^2$ is shown in Fig. 3 using the currently available F_2^γ measurements for 4 active flavours. The data are compared to the LO GRV and the SaS-1D parametrisations, and to a higher order (HO) prediction based on the HO GRV parametrisation for light quarks and on the NLO charm contribution calculated in Ref. 13. The data are measured in different x ranges. The comparison of the LO GRV curves for these x ranges shows that for $Q^2 > 100$ GeV^2 significant differences are expected. An augmented asymptotic prediction for F_2^γ is also shown. The contribution to F_2^γ from the three light flavours is approximated by Witten's leading order asymptotic form [11]. This has been augmented by adding a charm contribution evaluated from the Bethe-Heitler formula [14], and an estimate of the hadronic part of F_2^γ, which essentially corresponds to the hadronic part of the GRV (LO) parametrisation. In the region of medium x values studied here this asymptotic prediction in general lies higher than the GRV and SaS predictions but it is still in agreement with the data. The importance of the hadronic contribution to F_2^γ decreases with increasing x and Q^2, and it accounts for only 15 % of F_2^γ at $Q^2 = 59$ GeV^2 and $x = 0.5$.

As predicted by QCD the evolution of F_2^γ leads to a logarithmic rise with Q^2, but theoretical and experimental uncertainties are currently too large for a precision test

of perturbative QCD.

2.3. Azimuthal Correlations

Only the structure function F_2^γ has so far been determined directly from measurements of double-differential cross-sections for eγ events with hadronic or leptonic final states. It has been pointed out [15] that azimuthal correlations in the final-state particles from two-photon collisions are sensitive to additional structure functions. Azimuthal correlations can thus supplement the direct measurement of structure functions. ALEPH [16], L3 [17] and OPAL [18] have measured azimuthal correlations using single-tag $e^+e^- \to e^+e^-\mu^+\mu^-$ events.

For single-tag events two independent angles can be defined in the $\gamma\gamma^*$ centre-of-mass system assuming that the target photon direction is parallel to the beam axis: The azimuthal angle χ is the angle between the planes defined by the $\gamma\gamma^*$ axis and the two-body final state and the $\gamma\gamma^*$ axis and the tagged electron. The variable $\eta = \cos\theta^*$ is defined by the angle θ^* between the μ^- and the $\gamma\gamma^*$ axis.

Neglecting the longitudinal component of the target photon and setting $(1-y)$ to one, the cross-section can be written as ($F_2^\gamma = 2xF_T^\gamma + F_L^\gamma$):

$$\frac{\mathrm{d}\sigma(\mathrm{e}\gamma \to \mathrm{e}\mu^+\mu^-)}{\mathrm{d}x\mathrm{d}y\mathrm{d}\eta\mathrm{d}\chi/2\pi} = \frac{2\pi\alpha^2}{Q^2}\left(\frac{1+(1-y)^2}{xy}\right)\left[2x\tilde{F}_T^\gamma + \tilde{F}_L^\gamma - \tilde{F}_A^\gamma\cos\chi + \frac{\tilde{F}_B^\gamma}{2}\cos 2\chi\right]. \tag{3}$$

The conventional structure functions are recovered by integration over η and χ: $F_i^\gamma = \int_{-1}^{1}\int_0^{2\pi}\frac{d\chi d\eta}{2\pi}\tilde{F}_i^\gamma (i = 2, A, B)$. The structure functions F_T and F_L are related to the scattering of transverse and longitudinally polarized virtual photons, respectively. F_A is related to the interference terms between longitudinal and transverse photons and F_B to the interference term between purely transverse photons. The longitudinal structure function F_L^γ has been shown to be equal to the structure function F_B^γ in leading order and for massless muons, although coming from different helicity states of the photons.

The variation of F_A^γ and F_B^γ with x is in general consistent with QED (Figs. 4 and 5 and Ref. 18). The measured values are significantly different from zero. Apart from being an interesting test of QED, these results are especially important as a first step towards measuring the additional structure function for hadronic events using azimuthal

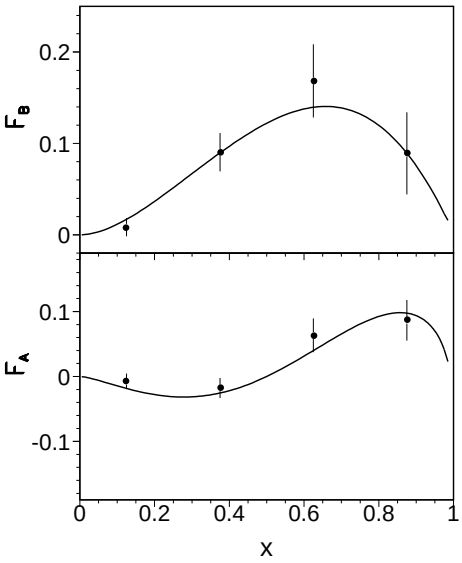

Figure 4: The structure functions F_B^γ and F_A^γ for the process $e^+e^- \to e^+e^-\mu^+\mu^-$ (L3). The lines show the QED expectation.

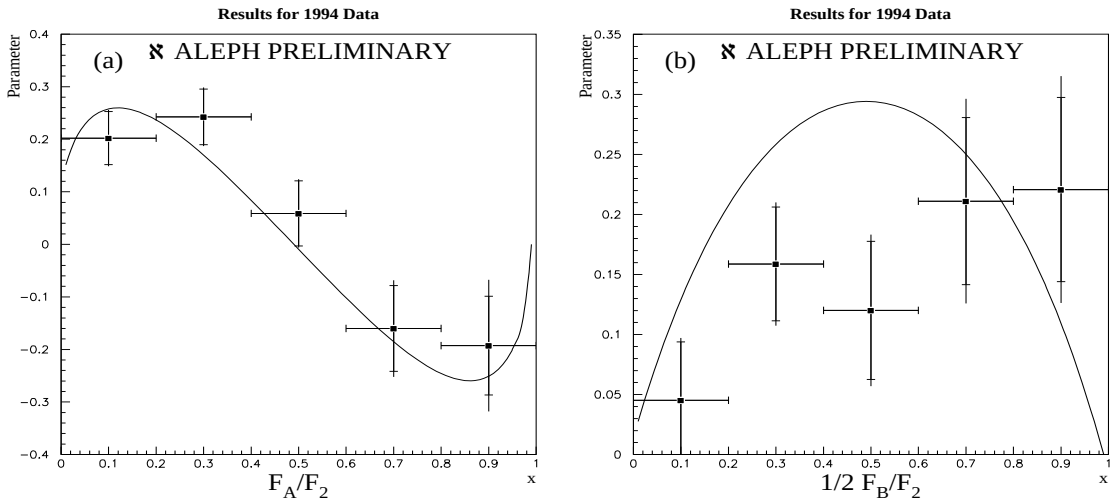

Figure 5: The ratio of structure functions, F_A^γ/F_2^γ and $1/2 \cdot F_B^\gamma/F_2^\gamma$, for the process $e^+e^- \to e^+e^-\mu^+\mu^-$ (ALEPH). The lines show the QED expectation.

correlations. Such a measurement will be much more difficult due to the problems related to the jet finding in hadronic events.

3. Photon–Photon Scattering

If both scattered electrons remain undetected, the Q^2 of the two interacting photons is very small and both photons can be considered to be quasi-real. At high $\gamma\gamma$ centre-of-mass energies $W = \sqrt{s}_{\gamma\gamma}$ the total cross-section for the production of hadrons in the interaction of two real photons is expected to be dominated by interactions where the photon has fluctuated into an hadronic state.

In LO QCD the $\gamma\gamma$ interactions can be classified by three different processes: direct, single- and double-resolved. The bare photons interact in the direct process, whereas in resolved events the partons (quarks or gluons) inside the hadronic state of the photon take part in the hard interaction. The probability to find partons in the photon is parametrised by the parton density functions.

3.1. Total Cross Sections

Measuring the $\sqrt{s}_{\gamma\gamma}$ dependence of the total $\gamma\gamma$ cross-section should improve our understanding of the hadronic nature of the photon and the universal high energy behaviour of total hadronic cross-sections.

The total cross-sections σ for hadron-hadron and γp collisions are well described by a Regge parametrisation of the form $\sigma = Xs^\epsilon + Ys^{-\eta}$, where $\sqrt{s}$ is the centre-of-mass energy of the hadron-hadron or γp interaction. The first term in the equation is due to Pomeron exchange and the second term is due to Reggeon exchange [19].

Assuming factorisation of the Pomeron term X, the total $\gamma\gamma$ cross-section can be related to the pp (or $\overline{\mathrm{p}}\mathrm{p}$) and γp total cross-sections at high centre-of-mass energies $\sqrt{s}_{\gamma\gamma}$ where the Pomeron trajectory should dominate:

$$\sigma_{\gamma\gamma} = \frac{\sigma^2_{\gamma\mathrm{p}}}{\sigma_{\mathrm{pp}}}. \tag{4}$$

A slow rise of the total cross-section with energy is predicted, corresponding to $\epsilon \approx 0.08$. This rise can also be attributed to an increasing cross-section for parton interactions leading to mini-jets in the final state [20].

Before LEP the total hadronic $\gamma\gamma$ cross-section has been measured by PLUTO [21], TPC/2γ [22] and the MD1 experiment [23]. These experiments have measured at centre-of-mass energies W below 10 GeV before the onset of the high energy rise of the total cross-section. Using LEP data taken at $\mathrm{e^+e^-}$ centre-of-mass energies $\sqrt{s}_{\mathrm{ee}} = 130 - 161$ GeV L3 [24] has demonstrated that the total hadronic $\gamma\gamma$ cross-section in the range $5 \leq W \leq 75$ GeV is consistent with the universal Regge behaviour of total cross-sections which was also observed in γp scattering at HERA. The L3 measurement is shown in Fig. 6 together with a preliminary OPAL measurement [25] in the range $10 < W < 110$ GeV using data taken at $\sqrt{s}_{\mathrm{ee}} = 161 - 172$ GeV. The observed energy dependence of the cross-section is similar, but the values for $\sigma_{\gamma\gamma}$ are about 20 % higher. It should be noted that the errors are strongly correlated between the W bins in both experiments. Furthermore, L3 has used the Monte Carlo generator PHOJET [28] for the unfolding, whereas for the OPAL measurement the unfolding results of PHOJET and PYTHIA are averaged. The unfolded cross-section using PHOJET is about 5 % lower than the central value. In both experiments the cross-sections obtained using PHOJET are lower than the cross-section obtained with PYTHIA.

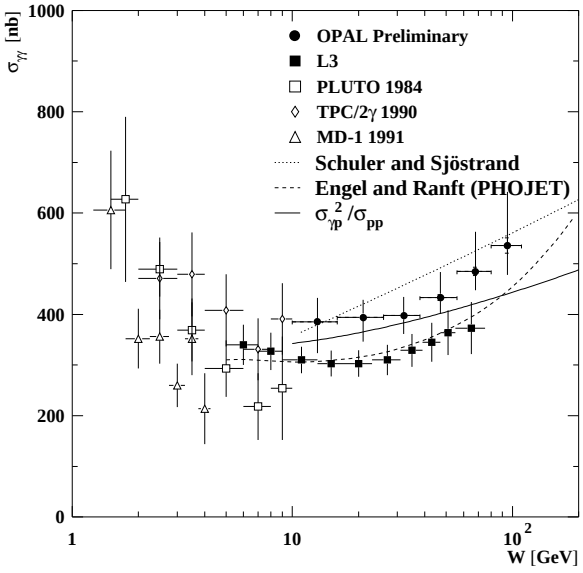

Figure 6: Total cross-section of the process $\gamma\gamma \to$ hadrons

The total cross-section is compared to several theoretical models. Based on the Donnachie-Landshoff model [26], the assumption of a universal high energy behaviour of $\gamma\gamma$, γp and pp cross-sections is tested. The parameters X and Y are fitted to the total $\gamma\gamma$, γp and pp cross-sections in order to predict $\sigma_{\gamma\gamma}$ via Eq. 4. This is done assuming that the cross-sections can be related at $\sqrt{s}_{\gamma\gamma} = \sqrt{s}_{\gamma\mathrm{p}} = \sqrt{s}_{\mathrm{pp}}$. The

process dependent fit values for X and Y are taken from Ref. 19 together with the values of the universal parameters $\epsilon = 0.0790 \pm 0.0011$ and $\eta = 0.4678 \pm 0.0059$. This simple ansatz gives a reasonable description of the total $\gamma\gamma$ cross-section $\sigma_{\gamma\gamma}$. Schuler and Sjöstrand [27] give a total cross-section for the sum of all possible event classes in their model of $\gamma\gamma$ scattering where the photon has a direct, an anomalous and a VMD component. They consider the spread between this prediction and the simple factorisation ansatz as conservative estimate of the theoretical band of uncertainty. The prediction of Engel and Ranft [28] is also plotted which is implemented in PHOJET. It is in good agreement with the L3 measurement and significantly lower than the OPAL measurement. The steeper rise predicted by Engel and Ranft is in agreement with both measurements.

A large part of the cross-section (about 20 % in both MC models) is due to diffractive and elastic events (e.g. $\gamma\gamma \to \rho\rho$). At high W the detectors have only little acceptance for these events and the correction procedure has to rely heavily on the MC model. In the future it will therefore be very important to gain a better understanding of these processes in $\gamma\gamma$ interactions.

3.2. Jet Production

The measurement of inclusive jet cross-sections and the comparison with NLO QCD calculations [29,30] and LO QCD Monte Carlo simulations using different parametrisations of the parton distributions of the photons can constrain the relatively unknown gluonic content of the photon.

In contrast to deep inelastic electron-photon scattering, which in leading order is only sensitive to the quark content of the photon, the gluon content of the photon can be tested, especially in the case of double-resolved processes, in the interaction of two almost real photons. Inclusive one-jet and two-jet cross-sections have been measured at an e^+e^- centre-of-mass energy of $\sqrt{s}_{ee} = 58$ GeV at TRISTAN [31,32] and at $\sqrt{s}_{ee} = 130 - 172$ GeV by OPAL [33,34]. In all cases the cone jet finding algorithm has been used.

In Fig. 7 the $E_T^{\rm jet}$ distribution measured by OPAL [34] at $\sqrt{s}_{ee} = 161 - 172$ GeV is compared to a NLO perturbative QCD calculation of the inclusive two-jet cross-section by Kleinwort and

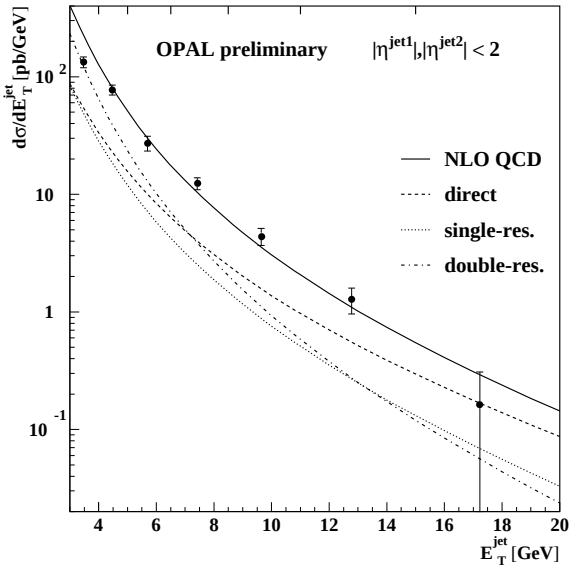

Figure 7: The inclusive two-jet cross-section as a function of $E_T^{\rm jet}$ for jets with $|\eta^{\rm jet}| < 2$ using a cone size $R = 1$.

Kramer [29] who use the NLO GRV parametrisation of the photon structure function [9]. The direct, single- and double-resolved parts and their sum are shown separately. The data points are in good agreement with the calculation except in the first bin where the calculation predicts a much higher cross-section. The resolved cross-sections dominate in the region $E_T^{\rm jet} \lesssim 8$ GeV, whereas, at high $E_T^{\rm jet}$ the direct cross-section is largest.

The NLO QCD calculation gives the jet cross-section for massless partons, whereas the experimental jet cross-sections are measured for hadrons. The difference due to fragmentation mainly contributes at low $E_T^{\rm jet}$ values. A correction to the parton level would increase the cross-section by about a factor of 1.2 to 1.3.

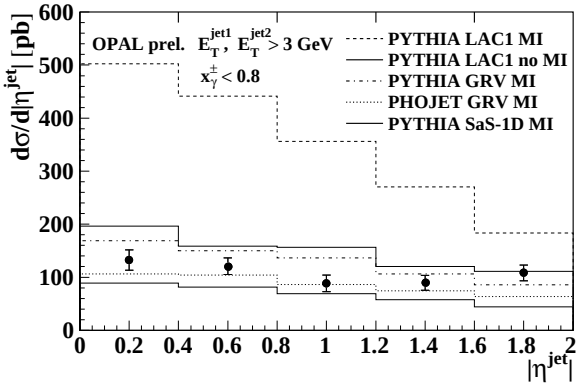

Figure 8: The inclusive two-jet cross-section as a function of $\eta^{\rm jet}$ for jets in mainly resolved event with $E_T^{\rm jet} > 3$ GeV using a cone size $R = 1$.

The inclusive two-jet cross-section as a function of $|\eta^{\rm jet}|$ is shown in Fig. 8 for events with a large double-resolved contribution after requiring $x_\gamma^\pm < 0.8$. The variable $x_\gamma^\pm$ specifies the fraction of the photon energy participating in the hard scattering:

$$x_\gamma^+ = \frac{\sum\limits_{\rm jets=1,2} (E + p_z)}{\sum\limits_{\rm hadrons} (E + p_z)} \quad \text{and} \quad x_\gamma^- = \frac{\sum\limits_{\rm jets=1,2} (E - p_z)}{\sum\limits_{\rm hadrons} (E - p_z)}, \tag{5}$$

where p_z is the momentum component along the z axis of the detector and E is the energy of the jets or hadrons. Ideally, for direct events without remnant jets $x_\gamma^+ = 1$ and $x_\gamma^- = 1$, whereas for double-resolved events both values x_γ^+ and x_γ^- are expected to be much smaller than 1.

The inclusive two-jet cross-section predicted by the two LO QCD Monte Carlo models, PYTHIA and PHOJET differ significantly even if the same photon structure function (here GRV LO) is used. This model dependence reduces the sensitivity to the parametrisation of the photon structure function. Different parametrisations were used as input to the PYTHIA simulation. The GRV-LO [9] and SaS-1D parametrisations [10] describe the data equally well, but LAC1 [35] which increases the cross-section for gluon-initiated processes overestimates the inclusive two-jet cross-section significantly. Turning off the simulation of multiple interactions (MI) within PYTHIA reduces the predicted cross-section using LAC1 by more than a factor of two.

For a more quantitative interpretation of these results in terms of parton distribution functions, it will be very important to understand the influence of multiple interactions on the jet cross-sections and to use jet definitions which will allow to compare theory (partons) and experiment (hadrons) directly. This is very similar to

the problems of measuring jet cross-sections in photoproduction at HERA discussed in these proceedings [36,37].

3.3. Charm Production

Similar to jet production, open charm production in photon-photon collisions can also be used to constrain the gluon content of the photon. The charm production cross-sections have been calculated in NLO [38,39]. The mass m_c of the charm quark sets the scale for the perturbative QCD calculation. The cross-section is factorized into the matrix elements for the production of heavy quarks and the parton densities for light quarks (q) and gluons. This 'massive' approach is expected to be valid if the transverse momenta p_T of the charm quarks are of the same order, $p_T \approx m_c$, which is true for the kinematic range probed at LEP. At LEP energies only the direct process $\gamma\gamma \to c\overline{c}$ and the single-resolved process $gq \to c\overline{c}$ are relevant.

The cleanest method to tag open charm is the reconstruction of $D^{*+} \to D^0\pi^+$ decays. Due to the small branching ratios of the D^0 into charged pions and kaons, this method is statistics limited. ALEPH has measured the charm cross-section using 33 ± 8 $D^{*\pm}$ mesons reconstructed in the LEP1 data. L3 has measured the charm cross-section in $\gamma\gamma$ interaction at LEP1 and LEP2 by tagging muons from semi-leptonic charm decays in the momentum range $2 < p_\mu < 7$ GeV/c at LEP1 and $2 < p_\mu < 15$ GeV/c at LEP2 [41]. The efficiency to tag muons is less than 10^{-3} leading to large systematic and statistical uncertainties.

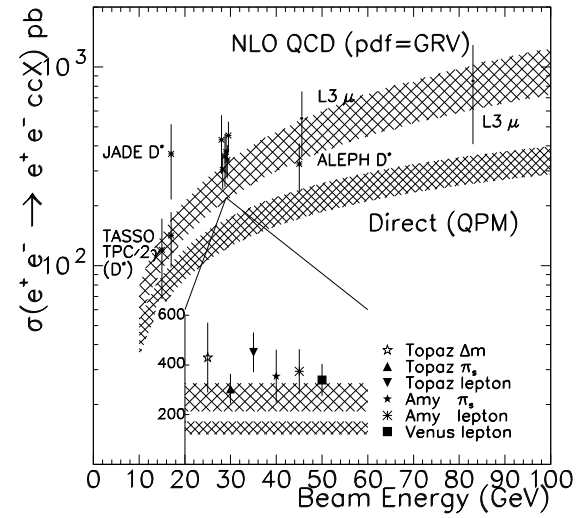

Figure 9: Cross-section for the process $e^+e^- \to e^+e^-c\overline{c}$ as a function of the electron beam energy.

The cross-section for the process $e^+e^- \to e^+e^-c\overline{c}$ as a function of the beam energy is shown in Fig. 9. The experimental results for various charm tagging methods used by pre-LEP experiments have been extrapolated to obtain a total charm cross-section [42]. The upper band shows the full NLO charm cross-section calculated by Drees et al [38] and the lower band the contribution from the Born term direct process (Quark Parton Model, QPM). The upper edge of the band is obtained by setting $m_c = 1.3$ GeV with a scale $\mu = m_c$ and the lower edge by setting $m_c = 1.7$ GeV with $\mu = \sqrt{2}m_c$. The data points obtained from the TRISTAN and JADE measurements cluster around the higher edge of the the 'massive' NLO calculation which uses the GRV parametrisation. At LEP ener-

gies the extrapolated measurement are in good agreement with the NLO calculation within the large errors.

4. Conclusions

Measurements of the photon structure function $F_2^\gamma(x, Q^2)$ from double-differential cross-section in eγ scattering mainly constrain the quark distribution in the photon. At low x LEP will be able to study the region where the onset of the rise of F_2^γ is expected from the HERA data on the proton structure function. LEP measurements will cover the kinematic range $x > 10^{-3}$ and $1 < Q^2 < 10^3$ GeV^2. A first measurement in the low x region has been presented by OPAL.

The logarithmic rise of F_2^γ with Q^2 for medium x and large Q^2 is observed as predicted, but theoretical and experimental uncertainties are currently too large for a precision test of perturbative QCD. The current systematic limitation of the F_2^γ measurements comes from the discrepancies between data distributions and Monte Carlo models for the hadronic final state. Work has started to improve the Monte Carlo models.

Azimuthal correlations have been used to determine the structure functions F_A and F_B in single-tagged $e^+e^- \to e^+e^-\mu^+\mu^-$ events. These structure functions correspond to different helicity states of the virtual photon and the target photon. The results are consistent with QED. In the future it will be interesting to extend these studies to hadronic final states.

First measurements by L3 and OPAL of the energy dependence of the total cross-section for hadron production in the interactions of quasi-real photons show the slow rise characteristic for hadronic interactions. However, the cross-section measured by L3 is about 20 % lower than the cross-section measured by OPAL.

Measurements of jet production in $\gamma\gamma$ interactions presented by OPAL disfavour parametrisations with a large gluon content in the photon like LAC1. The cross-sections are in good agreement with NLO calculations using the GRV parametrisation. Good agreement with the NLO calculation is also found for the measurement of the total charm production cross-section in $\gamma\gamma$ interactions by ALEPH and L3.

The experimental methods and the theoretical framework necessary for studying photon structure in the interactions of quasi-real photons at LEP and in photoproduction at HERA are very similar. This workshop has shown very clearly that both communities can learn a lot from each other.

5. Acknowledgements

I want to thank the Max-Planck-Institut für Physik and DESY, especially Bernd Kniehl, Gustav Kramer and Albrecht Wagner, for the excellent organisation of this

interesting workshop. Thanks also to the LEP collaborations for providing the plots.

6. References

1. OPAL Coll., K. Ackerstaff et al, *Z. Phys.* **C74** (1997) 33.
2. ALEPH Coll., paper submitted to Lepton-Photon 1997, LP-253.
3. I. Tyapkin, *proceedings of PHOTON '97*, Egmond aan Zee, The Netherlands (1997).
4. G. Marchesini et al., *Comp. Phys. Comm.* **67** (1992) 465.
5. T. Sjöstrand, *Comp. Phys. Commun.* **82** (1994) 74; T. Sjöstrand, LUND University Report, LU-TP-95-20 (1995).
6. ZEUS Coll., M. Derrick et al., *Phys. Lett.* **B354** (1995) 163.
7. J. Lauber et al., *proceedings of PHOTON '97*, Egmond aan Zee, The Netherlands (1997).
8. A compilation can be found in D. Morgan et al, *J. Phys. G*, *Nucl. Part. Phys.* **20** (1994) A1: PLUTO Coll., Ch. Berger et al., *Phys. Lett.* **B142** (1984) 111; PLUTO Coll., Ch. Berger et al., *Nucl. Phys.* **B281** (1984) 365; JADE Coll., W. Bartel et al., *Z. Phys.* **C24** (1984) 231; TASSO Coll., M. Althoff et al., *Z. Phys.* **C31** (1986) 527; TPC/2γ Coll., H. Aihara et al., *Z. Phys.* **C34** (1987) 1; AMY Coll., Y. Sasaki et al., *Phys. Lett.* **B252** (1990) 491; TOPAZ Coll., K. Muramatsu et al., *Phys. Lett.* **B332** (1994) 477; DELPHI Coll., P. Abreu et al., *Z. Phys.* **C69** (1996) 223 ($Q^2 = 12$ GeV^2); AMY Coll., T. Kojima et al., *Phys. Lett.* **B400** (1997) 395; ($Q^2 = 6.8$ GeV^2); OPAL Coll., K. Ackerstaff et al, *Z. Phys.* **C74** (1997) 33 ($Q^2 = 7.5, 14.7, 135$ GeV^2); OPAL Coll., K. Ackerstaff et al, CERN-PPE/97-87 ($Q^2 = 9, 14.5, 30, 59$ GeV^2); OPAL Coll., K. Ackerstaff et al, CERN-PPE/97-103 ($Q^2 = 1.86, 3.76$ GeV^2); ALEPH Coll., paper submitted to Lepton-Photon 1997, LP-315; DELPHI Coll., submitted to Lepton-Photon 1997 ($Q^2 = 6.3, 13, 22$ GeV^2).
9. M. Glück, E. Reya and A. Vogt, *Phys. Rev.* **D46** (1992) 1973; Phys. Rev. **D45** (1992) 3986.
10. G. A. Schuler and T. Sjöstrand, *Z. Phys.* **C68** (1995) 607.
11. E. Witten, *Nucl. Phys.* **B120** (1977) 189.
12. W. A. Bardeen and A. J. Buras, *Phys. Rev.* **D20** (1979) 166; *Phys. Rev.* **D21** (1980) 2041;
13. E. Laenen, J. Smith, S. Riemersma and W. L. van Neerven, *Phys. Rev.* **D49** (1994) 5753.
14. E. Witten, *Nucl. Phys.* **B104** (1976) 445.
15. C. Peterson et al., *Nucl. Phys.* **B229** (1983) 301; CELLO Coll., H.-J. Behrend et al., *Z. f. Phys.* **C43** (1989) 1; J. H. Field, *proceedings of Photon '95*, Sheffield, U.K., eds. D. J. Miller, S. L. Cartwright and V. Khoze, World Scientific, Singapore, 490 (1995); N. Arteaga et al., *proceedings of Photon '95*,

Sheffield, U.K.; Phys. Rev. **D52** (1995) 4920; *Phys. Rev.* **D53** (1996) 2854; P. Aurenche et al., in *Physics at LEP2*, CERN 96-01, p.301 (1996).
16. C. Brew et al., *proceedings of PHOTON '97*, Egmond aan Zee, The Netherlands (1997).
17. L3 Coll., paper submitted to EPS97, Jerusalem.
18. OPAL Coll., K. Ackerstaff et al, *Z. Phys.* **C74** (1997) 49.
19. R. M. Barnett et al., *Review of Particle Physics*, *Phys. Rev.* **D54** (1996) 1.
20. M. Drees and R. M. Godbole, *Nucl. Phys.* **B339** (1990) 355; J. R. Forshaw and J. K. Storrow, *Phys. Rev.* **D46** (1992) 4955; M. Drees and R. M. Godbole, *Z. Phys.* **C59** (1993) 591; A. Corsetti, R. M. Godbole, G. Panchieri, *proceedings of PHOTON '97*, Egmond aan Zee, The Netherlands (1997).
21. PLUTO Coll., Ch. Berger et al., *Phys. Lett.* **B149** (1984) 421.
22. TPC/2γ Coll., H. Aihara et al., *Phys. Rev.* **D41** (1990) 2667.
23. S. E. Baru et al., *Z. Phys.* **C53** (1992) 219.
24. L3 Coll., M. Acciarri et al., CERN-PPE/97-48.
25. F. Wäckerle, *proceedings of the XXVIII Int. Symposium on Multiparticle Dynamics*, Frascati, Italy (1997).
26. A. Donnachie and P. V. Landshoff, *Phys. Lett.* **B296** (1992) 227.
27. G. A. Schuler and T. Sjöstrand, *Z. Phys.* **C73** (1997) 677.
28. R. Engel and J. Ranft, *Phys. Rev.* **D54** (1996) 4244; R. Engel, *Z. Phys.* **C66** (1995) 203.
29. T. Kleinwort, G. Kramer, *Z. Phys.* **C75** (1997) 489; *Nucl. Phys.* **B477** (1996) 3; *Phys. Lett.* **B370** (1996) 141.
30. P. Aurenche et al., *Progr. Theor. Phys.* **92** (1994) 175.
31. AMY Coll., B. J. Kim et al., *Phys. Lett.* **B325** (1994) 248.
32. TOPAZ Coll., H. Hayashii et al., *Phys. Lett.* **B314** (1993) 149.
33. OPAL Coll., K. Ackerstaff et al., *Z. Phys.* **C73** (1997) 433.
34. OPAL Coll., paper submitted to Lepton-Photon 1997, LP-201;
35. H. Abramowicz, K. Charchula and A. Levy, *Phys. Lett.* **B269** (1991) 458.
36. J. Butterworth, hep-ex/9707001, these proceedings.
37. M. Klasen, hep-ph/9706292, these proceedings.
38. M. Drees, M. Krämer, J. Zunft, P. M. Zerwas, *Phys. Lett.* **B306** (1993) 371.
39. M. Cacciari, M. Greco, B. A. Kniehl, M. Krämer, G. Kramer, M. Spira *Nucl. Phys.* **B466** (1996) 173.
40. ALEPH Coll., *Phys. Lett.* **B355** (1995) 595.
41. L3 Coll., paper submitted to Lepton-Photon 1997, LP-092.
42. P. Aurenche et al., in *Physics at LEP2*, CERN 96-01, p.328 (1996) and references therein.